PROCEEDINGS, Eighteenth Workshop on Geothermal Reservoir Engineering
Stanford University, Stanford, California, January 26-28, 1993
SGP-TR-145

A FLUID PROPERTY MODULE FOR THE TOUGH2 SIMULATOR FOR SALINE BRINES WITH NON-CONDENSIBLE GAS

A. Battistelli (§), C. Calore (*), and K. Pruess (%)

(§) Aquater S.p.A. - ENI Group, 61047 S. Lorenzo in Campo (PS), Italy.
(*) Istituto Internazionale per le Ricerche Geotermiche - CNR, Piazza Solferino 2,56126, Pisa, Italy.
(%) Earth Sciences Division, Lawrence Berkeley Laboratory, Berkeley, CA, 94720.

ABSTRACT

A new equation-of-state module has been developed for the TOUGH2 simulator, belonging to the MULKOM family of computer codes developed at LBL. This EOS module is able to handle three-component mixtures of water, sodium chloride, and a non-condensible gas. It can describe liquid and gas phases, and includes precipitation and dissolution of solid salt.

The dependence of density, viscosity, enthalpy, and vapor pressure of brine on salt concentration is taken into account, as well as the effects of salinity on gas solubility in the liquid phase and related heat of solution. The main assumptions made in developing this EOS module are discussed, together with the correlations employed to calculate the thermophysical properties of multiphase multicomponent mixtures.

At present the non-condensible gas can be chosen to be air, CO_2, CH_4, H_2, or N_2. This paper focuses on H_2O-NaCl-CO_2 mixtures and describes new correlations obtained from fitting of published experimental data.

Illustrative results for geothermal reservoir depletion in the presence of salinity and non-condensible gas are presented. We demonstrate and analyze effects of vapor pressure lowering and gas solubility decrease from salinity, and loss of reservoir porosity and permeability from salt precipitation during boiling of brines.

INTRODUCTION

The thermodynamic and transport properties of geothermal fluids are very important for determining the natural state of a geothermal system and its behaviour under exploitation. Such fluids consist usually of complex mixtures of water, non-condensible gases (NCG) and salts dissolved in the liquid phase. As water always represents the main mixture component, its thermophysical properties are customarily used to model geothermal reservoirs. In some cases the content of other components is such that they can alter the reservoir performance significantly. The effects of CO_2 have been analyzed with numerical studies by several authors. The importance of salt content has not received as much attention in reservoir modeling, mainly because only a few high salinity reservoirs have been exploited up to now.

Even though the main effects of dissolved solids and NCG on fluid mixture properties are well-known, the quantitative evaluation of the effect of variable proportion of both salinity and NCG on reservoir conditions and performance requires additional studies.
For the compositional simulation approach required to study high-salinity natural systems containing also NCG, an EOS module for the LBL's multipurpose TOUGH2 numerical simulator has been developed.

MODELING APPROACH

The TOUGH2 code implements the general MULKOM architecture for coupled multiphase, multicomponent fluid and heat flows (Pruess, 1983, 1991a). This new EOS module has been developed to simulate flow problems in which the transport of a variable salinity brine and a NCG occurs.
In this formulation the multiphase system is assumed to be composed of three mass components: water, sodium chloride and CO_2, or some other NCG. Whereas water and the NCG components may be present only in the liquid and gas phases, the salt component may be present dissolved in the liquid phase or precipitated to form a solid salt phase. The solubility of NaCl in the gas phase is neglected.

The three mass components formulation employed has been developed by enhancing an already existing EOS module for simulating the non- isothermal flow of saline water and air (Pruess, 1991b). The treatment of precipitation/dissolution of sodium chloride has been introduced using the method employed to treat similar phenomena occurring for water-silica mixtures (Verma and Pruess, 1988). The reduction of rock porosity because of salt precipitation is taken into account, as well as the related decrease of formation permeability.
The formulation of H_2O-CO_2 fluid mixture basically follows that described by O'Sullivan et al. (1985). The

dependence of brine thermophysical properties on salt concentration has been included following an updated version of the thermophysical package developed by Aquater for a wellbore numerical simulator (Battistelli, 1991).
All relevant thermophysical properties are evaluated using a subroutine by subroutine structure, so that the correlations employed at present can be easily modified.

The dependence of brine enthalpy, density, viscosity and vapor pressure on salt concentration has been accounted for, as well as the effect on NCG solubility and heat of solution in the brine. Transport of the mass components occurs by advection in liquid and gas phases; binary diffusion in the gas phase for steam and the NCG is accounted for. Diffusive and dispersive processes in the liquid phase are not included in the present TOUGH2 code formulation. It is assumed that the three phases (gas, liquid, and solid) are in local chemical and thermal equilibrium and that no chemical reactions take place other than interphase mass transfer.

In the integral finite differences formulation used by TOUGH2, the mass balance equations are written in the following general form (Pruess, 1991a):

$$\frac{d}{dt}\int_{Vn} M^{(k)}\, dV = \int_{\Gamma n} \mathbf{F}^{(k)} \bullet \mathbf{n}\, d\Gamma + \int_{Vn} Q^{(k)} dV \qquad (1)$$

where k=1,2,3, indicates water, NaCl and NCG components, respectively. A complete description of the nomenclature used is given at the end of the paper. The accumulation and mass flux terms for the NaCl component (k=2) are written as follows:

$$M^{(2)} = \phi\, S_s\, \rho_s + \phi\, S_l\, \rho_l\, X_l^{(2)} \qquad (2)$$

$$\mathbf{F}^{(2)} = -\,k\,\frac{k_{rl}}{\mu_l}\,\rho_l\, X_l^{(2)}\,(\,\mathbf{grad}P_l - \rho_l\,\mathbf{g}\,) \qquad (3)$$

where S_s is the "solid saturation", defined as the fraction of pore volume occupied by solid salt.

THERMODYNAMIC PACKAGE DESCRIPTION

The primary variables used for single phase conditions are total pressure of reference phase, P, salt mass fraction, $X^{(2)}$, NCG mass fraction, $X^{(3)}$, and temperature, T. If the solid salt is present, the second primary variable is switched to solid saturation S_s. In two-phase conditions the third primary variable is switched from NCG mass fraction to gas phase saturation S_g.

Mass balances of water, salt and NCG components, together with the heat balance, are set up and solved by TOUGH2 using the Newtown-Raphson iteration method. During the iteration process, the EOS module must be capable of recognizing the appearance and disappearance of phases, and of providing all thermophysical properties of phases present, pertaining to the last updated primary variables. A description of the main tests performed to recognize the phase transitions and of the equations used to calculate phases properties is given below.

Liquid conditions

First the test for phase change to two-phase conditions is made checking if total pressure exceeds the boiling pressure of fluid mixture:

$$P \overset{?}{\geq} P_{boil}(T, X_l^{(2)}, X_l^{(3)}) \qquad (4)$$

The liquid phase boiling pressure is calculated according to:

$$P_{boil} = P_{b\ sat}(T, X_l^{(2)}) + P^{(3)}(T, X_l^{(2)}, X_l^{(3)}) \qquad (5)$$

If the test fails, a change to the two-phase state is made initializing the gas phase saturation to a small non zero quantity. The bubbling pressure of NCG, $P^{(3)}$, is calculated according to Henry's law and accounting for the salting-out effect.

The solid salt phase appears if the salt mass fraction in the liquid phase exceeds the halite solubility. If:

$$X_l^{(2)} > X^{(2)}{}_{sol}(T) \qquad (6)$$

precipitation starts and the second primary variable is switched from salt mass fraction $X^{(2)}$ to "solid saturation" S_s. (Actually, $10+S_s$ is then used as second primary variable, so that by the fact that this is large than 1 it can be distinguished from mass fractions, which are always between 0 and 1) When Eq. (6) indicates that precipitation is starting S_s is initialized to a small non zero value. Conversely, when solid phase is present, its disappearance is recognized simply by $S_s<0$. In this case the second primary variable is switched back to $X^{(2)}$, and is initialized with a value slightly smaller than the equilibrium solubility $X_{sol}^{(2)}(T)$.

The thermophysical properties of the liquid phase are calculated as follows. The density and viscosity are assumed to be the same as those for brine, with the assumption that the effect of dissolved gas can be neglected because of low gas solubility. Liquid phase density, viscosity and enthalpy are given by:

$$\rho_l = \rho_b(P, T, X_l^{(2)}) \qquad (7)$$

$$\mu_l = \mu_b(P, T, X_l^{(2)}) \qquad (8)$$

$$H_l = (1-X_l^{(3)})\, H_b(P, T, X_l^{(2)}) + X_l^{(3)}\, H_l^{(3)}(P^{(3)}, T) \quad (9)$$

Gas conditions

In single-phase gas conditions the salt component can be present only as solid precipitate, having neglected its (very small) solubility in the gas phase. The appearance of the liquid phase is tested checking the partial pressure of steam, $P^{(1)}$, against the vapor brine pressure:

$$P^{(1)} \overset{?}{<} P_{b\ sat}(T, X^{(2)}_{eq}) \quad (10)$$

The brine vapor pressure is calculated using $X^{(2)}_{eq} = 0$ if no solid phase is present in the element, otherwise it is assumed to be the solubility of NaCl at element temperature. Partial pressure of water component is calculated using an iterative procedure from total pressure, temperature and NCG mass fraction. If the above test fails, a transition to two-phase conditions is diagnosed, initializing the third variable as a gas phase saturation slightly lower than one.

Density, enthalpy and viscosity of single-phase gas fluid mixtures are calculated as follows:

$$\rho_g = \rho_g^{(1)}(P^{(1)}, T) + \rho_g^{(3)}(P^{(3)}, T) \quad (11)$$

$$H_g = (1-X_g^{(3)})\, H_g^{(1)}(P^{(1)}, T) + X_g^{(3)}\, H_g^{(3)}(P^{(3)}, T) \quad (12)$$

$$\mu_g = (1-X_g^{(3)})\, \mu_g^{(1)}(P^{(1)}, T) + X_g^{(3)}\, \mu_g^{(3)}(P^{(3)}, T) \quad (13)$$

Liquid-gas mixtures

For elements with two-phase fluid the phase transition test is made checking the gas phase saturation that is used as third primary variable. If $S_g \geq 1 - S_s$, then the liquid phase disappears and a transition to single-phase gas conditions is made. If $S_g \leq 0$, then the gas phase disappears and a transition to single-phase liquid conditions is made. Appearance or disappearance of a precipitated solid phase is handled as in liquid conditions.

With the assumption of additivity of partial pressures, the partial pressure of NCG is given by:

$$P^{(3)} = P - P_{b\ sat}(T, X_l^{(2)}) \quad (14)$$

The mole fraction of NCG in the liquid phase is calculated according to Henry's law:

$$Y_l^{(3)} = P^{(3)} / K_{hb}(T, m) \quad (15)$$

where m is the salt molality. Then the mass fraction of NCG in the liquid phase is calculated in an obvious way. The mass fraction of NCG in the gas phase is calculated from the density of fluid mixture, computed considering an ideal mixture of steam and gas:

$$\rho_g = \rho_g^{(1)}(P_{b\ sat}, T) + \rho_g^{(3)}(P^{(3)}, T) \quad (16)$$

then:

$$X_g^{(3)} = \rho_g^{(3)} / \rho_g \quad (17)$$

The specific enthalpy and viscosity of vapor phase are calculated using Eq. 12 and 13 respectively, with $P^{(1)} = P_{b\ sat}$.
The density, viscosity and enthalpy of liquid phase are calculated with Eq. 7, 8 and 9 respectively, using the component mass fractions in the liquid phase.

THERMODYNAMIC PROPERTIES OF MIXTURE COMPONENTS

The correlations used to evaluate the thermophysical properties of mixture components are described below. References are given for all those correlations available in the technical literature, whereas new correlations obtained through the regression of published experimental data are presented in detail.

Water and salt component properties

The pure water properties are always computed using the International Formulation Committee (1967) correlations implemented in the TOUGH2 code.

- **Brine vapor pressure.** The vapor pressure of sodium chloride solutions is calculated according to the equation presented by Haas (1976). It can be used in the temperature range from -11 to 300 °C; as stated by Haas, extrapolation to 325°C still seems acceptable. The salt content can range from 0 to halite saturation. The equations implemented differ from the original ones used by Haas as the IFC correlation has been used to compute pure water saturation pressure. Figure 1 shows the vapor saturated brine pressure vs temperature at different NaCl mass fractions.
It is seen that dissolved solids generally reduce the vapor pressure. The salinity-induced vapor pressure lowering (VPL) effects can be large, reducing vapor pressure to as little as 2/3 of the vapor pressure of pure water. To put this number in perspective, it is of interest to make a comparison with VPL effects from capillarity and adsorption-induced suction pressure. From the data given by Pruess and O'Sullivan (1992) it can be seen that a reduction of vapor pressure to 2/3 of the value for "bulk" pure water would require extremely strong suction pressures approaching -100 MPa! Thus it appears that salinity-induced VPL effects are likely to be more important in the depletion of

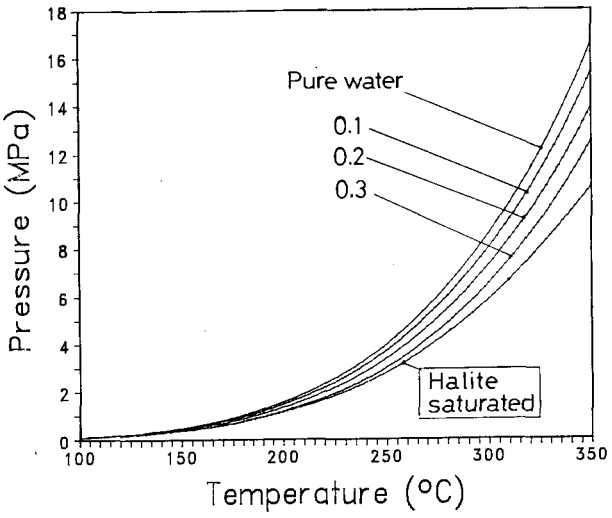

Figure 1. Vapor pressure of NaCl solutions from 0 mass fraction to halite saturation at 100° to 350°C.

vapor-dominated reservoirs than the capillarity/ adsorption induced effects.

- **Brine density.** The density of vapor-saturated brine is calculated using the equations presented by Haas (1976). They can be applied in the temperature range from 75 to 325 °C whereas the salt content can vary from 0 to 7.3 molal, or up to halite saturation if the corresponding molal concentration is lower. The density of vapor-saturated pure water is computed using the IFC formulation.
The effect of pressure on brine density is estimated with the assumption that brine compressibility is the same as that of pure water from the vapor-saturated pressure to current pressure.

- **Brine enthalpy.** The enthalpy of vapor-saturated sodium chloride solutions is calculated using the correlation of Michaelides (1981) based on the thermodynamic data presented by Silvester and Pitzer (1976). The corrections of typing errors in the Michaelides paper, presented by Gudmundsson and Thrainsson (1989), have been considered. The correlation should be applied in the temperature range from 100 to 300 °C. The compressed brine enthalpy is estimated assuming a similar pressure dependence for brine and pure water.

- **Brine viscosity.** The dynamic viscosity of vapor-saturated brine for salt mass fraction up to 0.30, is estimated using an equation quoted by Chierici et al. (1981), which applies a correction as a function of salt mass fraction to the dynamic viscosity of vapor saturated pure water. The latter is computed according to the IFC formulation.
The dynamic viscosity of compressed brine is calculated assuming a similar pressure dependence for brine and pure water.

- **Halite solubility.** The concentration of solutions that are both vapor- and halite-saturated is evaluated using an equation due to Potter and quoted by Chou (1987), who recommends the use of this equation from 0 to 382 °C.

- **Density and enthalpy of halite.** The density of halite is considered independent on pressure and temperature: a constant value of 2160 kg/m^3 is used (Deer et al., 1966).
The enthalpy of halite is calculated integrating the equation of heat capacity at constant pressure reported by Silvester and Pitzer (1976). The equation is valid from 25 to 800 °C (Palaban and Pitzer, 1987).

Carbon dioxide component

The equations used to calculate the carbon dioxide thermodynamical and transport properties are given below. A similar approach can be followed for other gases: this has already been done for air, methane, hydrogen and nitrogen.

- **Density and enthalpy of gaseous carbon dioxide.** The density and enthalpy of CO_2 as a function of temperature and its partial pressure are calculated from equations reported by Sutton and McNabb (1977). These equations are already used by the H_2O-CO_2 EOS module described by O'Sullivan et al. (1985).

- **Viscosity of gaseous carbon dioxide.** The CO_2 dynamic viscosity is calculated using the correlation quoted by Pritchett et al. (1981) and already implemented in the TOUGH2 H_2O-CO_2 EOS module.

- **Henry's law constant.** Dissolution of carbon dioxide in pure water and sodium chloride brines is described using Henry's law and the concept of salting-out; the Henry's constant is then calculated as:

$$K_{hb}(T, X_l^{(2)}) = K_h(T)\ 10^{(\ m\ k_b(T)\ )} \qquad (18)$$

where k_b is the salting-out coefficient. Several approximations are implicit in this formulation: the most important is the application of the formula at other than very small solute gas concentrations. Henry's law constant for the dissolution of carbon dioxide in pure water and the salting-out coefficient are calculated using polynomial regressions of data from 0 to 300 °C published by Cramer (1982). To extend the temperature range of Henry's constant correlation, the values reccomended by D'Amore and Truesdell (1988) from 300 °C to the critical point of water were also considered. The polynomial fit of Henry's constant is shown in Figure 2. The standard deviation is 4.74 MPa. The equation is as follows:

$$K_h(T) = \sum_{i=0}^{5} [\ A(i)\ T^i\ ] \qquad (19)$$

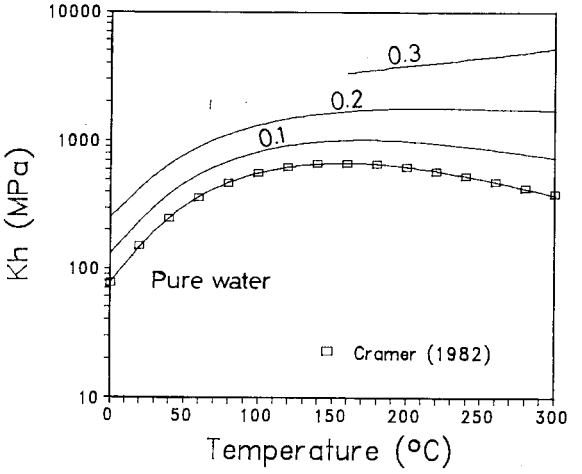

Figure 2. Henry's law constant for CO_2 in NaCl solutions from 0 to 0.3 mass fraction at 0° to 300°C.

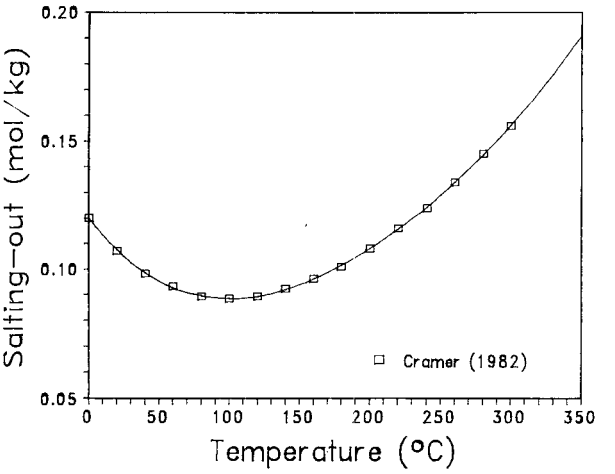

Figure 3. Salting-out coefficient for CO_2 dissolved in NaCl solutions from 0° to 350°C.

where the coefficients A(i) have the following values:

A(0) = 7.83666 E+8
A(1) = 1.96025 E+6
A(2) = 8.20574 E+4
A(3) = -7.40674 E+2
A(4) = 2.18380 E+0
A(5) = -2.20999 E-3

The equation for the salting-out coefficient is:

$$k_b(T) = \sum_{i=0}^{4} [\, B(i)\, T^i \,] \qquad (20)$$

The polynomial fit is shown in Figure 3. Standard deviation is 3.09 E-4 kg/mol. The coefficients B(i) have the following values:

B(0) = 1.19784 E-1
B(1) = -7.17823 E-4
B(2) = 4.93854 E-6
B(3) = -1.03826 E-8
B(4) = 1.08233 E-11

- Enthalpy of dissolved carbon dioxide. The enthalpy of carbon dioxide dissolved in pure water is calculated adding the heat of solution to the enthalpy of carbon dioxide in the gaseous state, according to the expression:

$$H_l^{(3)}(P^{(3)}, T) = H_g^{(3)}(P^{(3)}, T) + \Delta H_{sol}^{(3)}(T) \qquad (21)$$

The heat of solution can be calculated using the expression of temperature dependence of the equilibrium constant for the chemical reaction of solution:

$$CO_{2\,(g)} \text{---} > CO_{2\,(l)}$$

The equation that relates the heat of solution of a gas to its Henry's constant has been presented, among others, by Himmelblau (1959):

$$\left(\frac{\delta \ln K_h(T)}{\delta T}\right)_p = -\frac{\Delta H_{sol}^{(3)}(T)}{R\ TK^2} W^{(3)} \qquad (22)$$

In the above equation the molecular weight $W^{(3)}$ of CO_2 has been added to convert the heat of solution from J/mol to J/kg units. Eq. (22) is used to derive the heat of solution for carbon dioxide in sodium chloride brines using the Henry's constant K_{hb} given by Eq. (18). Figure 4 shows the heat of solution of CO_2 as a function of temperature at different salt mass fractions.

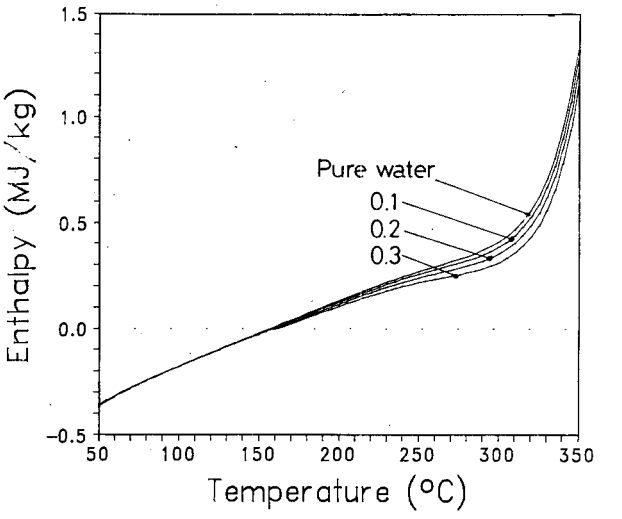

Figure 4. Heat of solutions for CO_2 dissolved in NaCl solutions from 0 to 0.3 mass fraction at 50° to 350°C.

NUMERICAL SIMULATIONS

It is well known that the main effects of solids dissolved in the liquid phase are the decrease of vapor pressure and enthalpy, and the increase of density and viscosity in the liquid phase. Furthermore, the NCG solubility in the liquid brine decreases (salting-out effect). We have performed numerical simulations to show some of the capabilities of the new EOS module to model the effects of dissolved solids and NCG on the behavior of geothermal reservoirs. For this purpose the examples presented are not designed to represent site-specific cases.

Depletion of zero-dimensional reservoir

The first simulations consider constant rate production from a zero-dimensional 'lumped-parameter' reservoir model in order to show the effects of salinity and CO_2 due to differences in the thermodynamic properties and mobilities of liquid and gas phases.

A block of 1 km^3 volume is considered initially in single-phase liquid conditions with a temperature of 260 °C and a pressure of 8 MPa. The formation parameters are the following: rock grain density 2600 kg/m^3, rock specific heat 920 J/(kg °C), formation thermal conductivity 2.51 W/(m °C), rock porosity 5%, Corey's relative permeability curves with residual liquid saturation of 0.3 and residual gas phase saturation of 0.05. Capillary pressure effects and VPL due to suction pressure are not included. Production occurs at a constant rate of 41.5 kg/s to attain the complete depletion in about 30 years when the block is filled with pure water.

A first series of simulations considers the two-component H_2O-NaCl system with salt mass fraction of 0 (pure water case), 0.01, 0.05, 0.10, 0.20 and 0.30 respectively. Figure 5 shows the pressure during block depletion as a function of time for the six cases. The time necessary for complete fluid depletion increases with increasing NaCl content as the fluid reserves stored initially increase from 39.41 E+9 kg for the pure water case up to 53.05 E+9 kg for the 0.30 salt mass fraction case. Two-phase conditions develop in the block for all cases within a few months; the boiling of fluid occurs at different pressure because of VPL due to salinity. Then the pressure remains almost constant for about 10 to 13 years until the gas phase mobility increases as shown by the enthalpy of produced fluid (Fig. 6). In this period the salinity of the reservoir liquid phase is almost constant (Fig. 7) as the salt mass

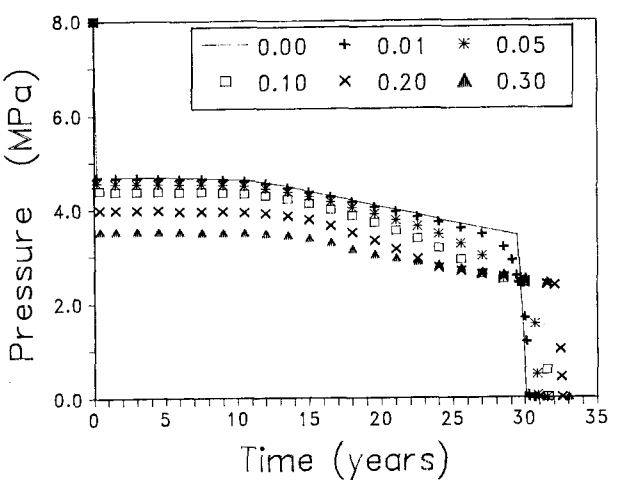

Figure 5. Depletion of zero-dimensional reservoir at different NaCl mass fractions for the H_2O-NaCl mixture.

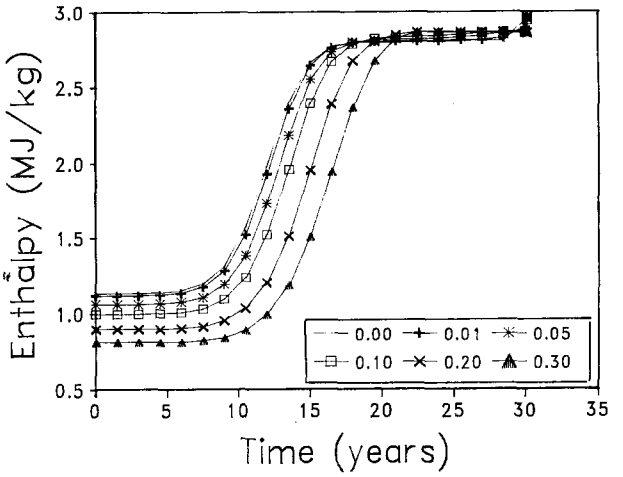

Figure 6. Production enthalpy as a function of time during reservoir depletion.

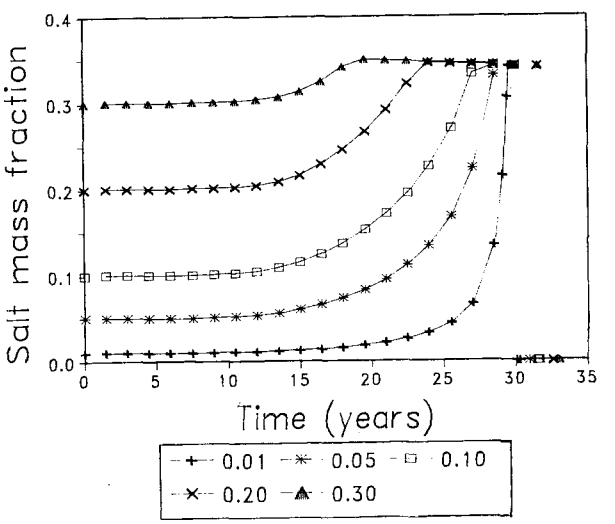

Figure 7. NaCl mass fraction in the liquid phase as a function of time during reservoir depletion.

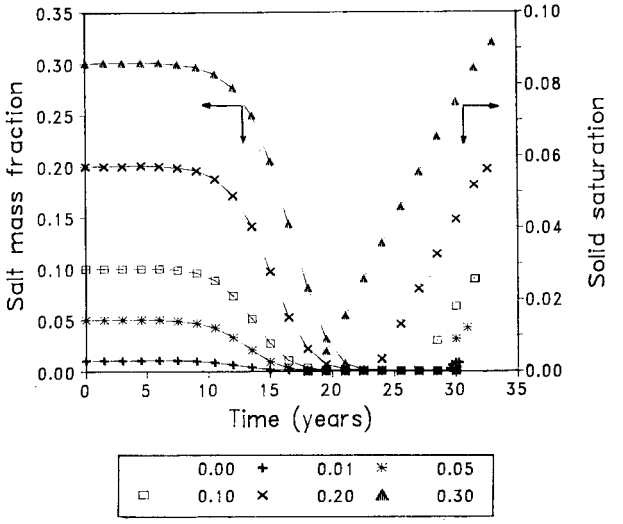

Figure 8. NaCl mass fraction in produced fluid and solid saturation as a function of time during reservoir depletion.

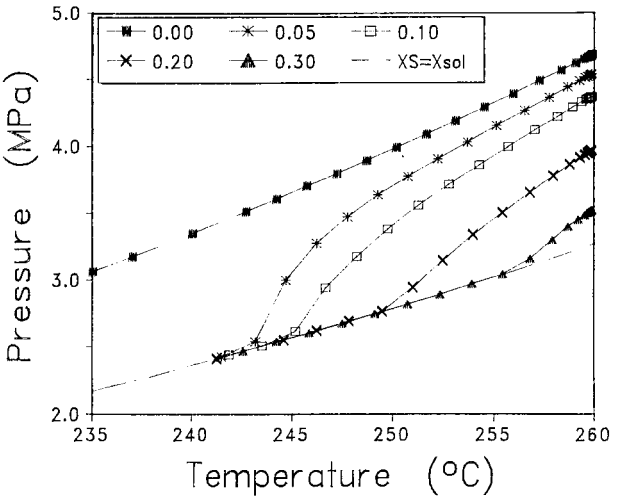

Figure 9. Brine vapor pressure as a function of reservoir temperature during reservoir depletion.

fraction in the produced fluid (Fig. 8).

The increase of gas phase mobility determines the rise of produced fluid enthalpy; then the reservoir temperature starts to decline significantly, also reducing reservoir pressure. The salt mass fraction in produced fluid declines as it can be extracted only dissolved in the less mobile liquid phase. This and the continous vaporization of water in the liquid phase determines the increase of salt concentration until it equals the halite solubility. Obviously the precipitation of solid salt occurs earlier depending on the initial salt content (see Figure 8). Figure 7 shows that for a complete drying process a solid salt phase can develop even for a very low initial salt concentration; in this case the increase of liquid phase salinity occurs close to the complete vaporization of liquid phase.

Figure 5 shows the pressure decline due to both temperature decline and salinity increase; when solid salt is present, the pressure becomes almost the same for the different cases because the salt mass fraction in the liquid phase is controlled by the solubility of halite and reservoir temperature differs only slightly. Figure 9 shows the brine vapor pressure as a function of reservoir temperature for the two-phase mixture. It shows the maximum VPL due to salt content, which is limited by the presence of solid salt phase.

Because of different initial fluid reserves, the liquid phase disappears over longer periods as the initial salt content increases. The increase in reservoir life is not proportional to the initial fluid reserves, as more and more salt is precipitated to form the solid phase that cannot be produced.

The second series of simulation considers the previous cases with the addition of 0.002 (2000 ppm) CO_2 mass fraction to the fluid mixture. The effect of NCG on reservoir pressure decline is shown in Figure 10. The salting-out effect increases the CO_2 bubbling pressure: up to a salt content of about 0.10 this increase balances the VPL. Then the increase of CO_2 bubbling pressure is higher and the fluid boiling pressure increases. Initial pressure depletion is governed by the exsolution of CO_2 from the liquid phase. The partial pressure of NCG declines as soon as the gas phase forms, as the NCG is partitioned preferentially in the gas phase. After 1.5 years, the NCG mass fraction into the gas phase is about 0.13 for the zero salinity case, but rises to 0.60 for the highest salinity. Figure 11 shows the decrease of NCG mass fraction in the liquid phase due to increasing salt contents. Considering the production characteristics, this effect determines a lower NCG content in produced fluid, as the low gas content liquid phase is initially produced (see Figure 12).

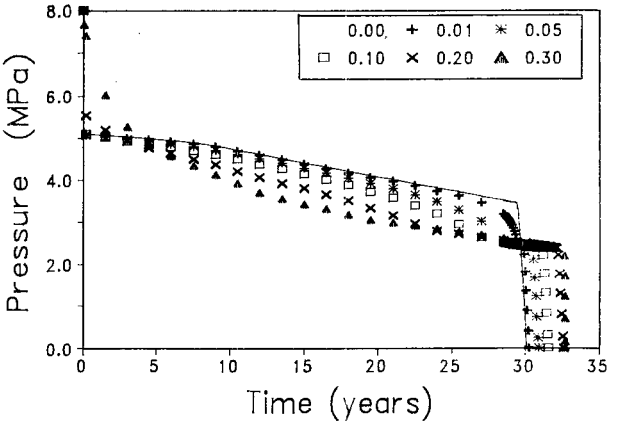

Figure 10. Depletion of zero-dimensional reservoir at different NaCl mass fractions in the presence of 2,000 ppm of CO_2.

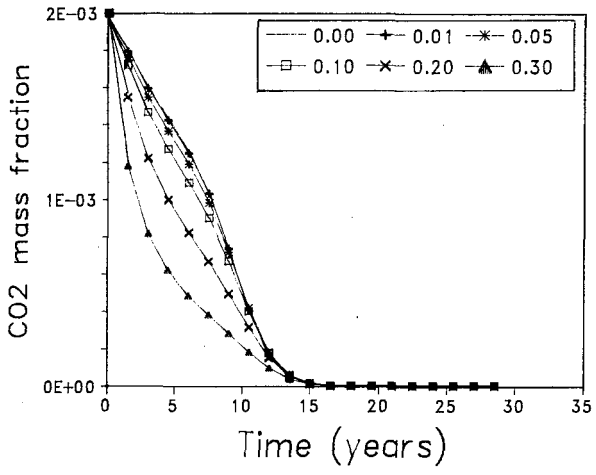

Figure 11. CO_2 mass fraction in the liquid phase as a function of time during reservoir depletion.

When its mobility increases, the rich NCG vapor phase is produced determining the sharp increase of NCG in produced fluid with higher concentrations for higher salt content; the position of maximum CO_2 mass fraction is also dependent on the salt content. Then the NCG declines with time and after about 15 years the carbon dioxide content in the liquid phase becomes negligible.
As expected, with respect to the previous series of simulations, the addition of NCG affects the initial reservoir pressure depletion until the partial pressure of NCG declines. These effects are concentrated in the first 10 years; after 15 years the pressure decline for all the cases is coincident to that of corresponding free-gas case.

For the parameters used in these simulations, excluding the last depletion period when the liquid phase is almost

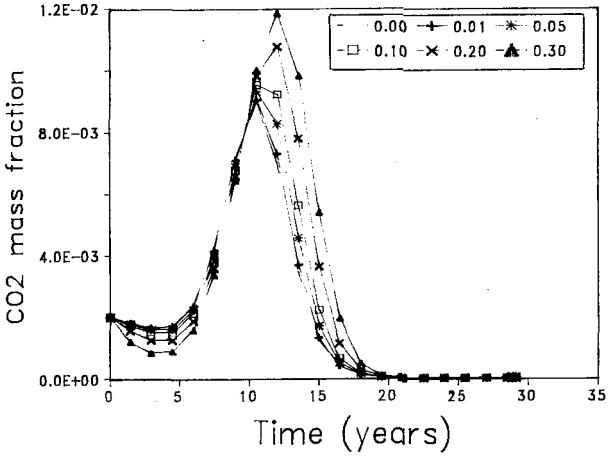

Figure 12. CO_2 mass fraction in produced fluid as a function of time during reservoir depletion.

completely vaporized, the effect of salt becomes important when its initial concentration exceeds about 50,000 ppm. The main effects on production characteristics are lower enthalpy and lower reservoir pressure for the cases with higher salinity; both can be considered as negative features of reservoirs containing brine.

Depletion of tight matrix blocks

We have simulated fluid production from tight matrix blocks under conditions considered representative of vapor dominated systems to show some effects of VPL and permeability reduction due to salinity.
Changes in formation permeability due to precipitation or dissolution of sodium chloride are modeled in the present EOS module formulation using the porosity-permeability correlations given in the paper by Verma and Pruess (1988). We used the 'series model' for tubular flow for the simulations presented here, with fractional lenght=0.8 and critical porosity fraction=0.8.

We have used the same model system as previously studied by Pruess and O'Sullivan (1992). The model consists of a single cubic block of rock matrix with side lenght D=50 m, surrounded by fractures wich have a fractional volume of 1E-4. The matrix block is discretized according to the MINC method (Pruess and Narasimhan, 1985) with 9 nested cubes of 2%, 4%, 6%, 8%, 10%, 13%, 16%, 20%, and 21% volume fractions. Matrix permeability and porosity are 5 E-18 m^2 and 5%, respectively. Liquid relative permeability and capillary pressure are taken as the van Genuchten form. Gas relative permeability is given by $k_{rg}=1-k_{rl}$. VPL due to suction pressure effects is not included. The system is initially in two-phase conditions at temperature of 240 °C, with liquid saturation of 80% in the matrix block, and 1% in the fractures.
Block depletion occurs by a 'well' on deliverability placed in the fractures (bottomhole pressure of 1 MPa, productivity index of 1.788E-13 m^3). Additional parameter specifications are given in the paper by Pruess and O'Sullivan (1992).

Three different cases were simulated: (Case 1) reservoir fluid is pure water; (Case 2) liquid phase is a brine with 0.20 salt mass fraction; (Case 3) same as Case 2 but permeability reduction due to salt precipitation is considered. Initial fluid pressure is 3.348 MPa for Case 1 and 2.838 MPa for Cases 2 and 3 because of VPL effects due to brine salinity. Initial fluid reserves are 4.089E+6 kg for Case 1, and 4.948E+6 kg (of which 3.962E+6 kg is water) for Cases 2 and 3.

Figure 13 shows the well production as a function of time for the 3 cases. The higher production rate for Case 1 occurs because of the higher initial pressure in the system; this causes a faster recovery of fluid

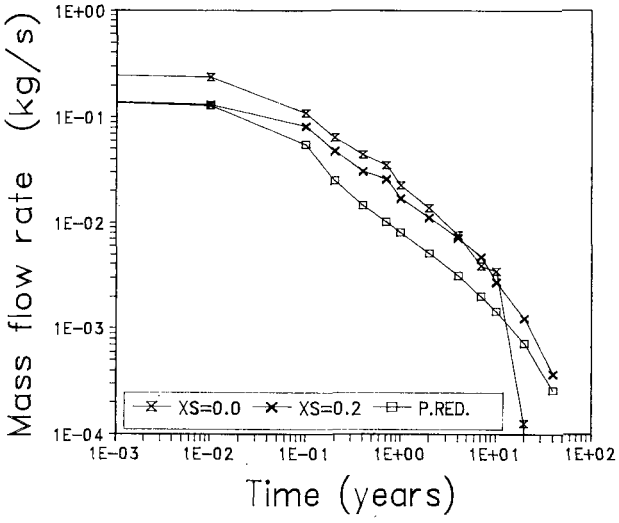

Figure 13. Production flow rate as a function of time during depletion of a tight matrix block.

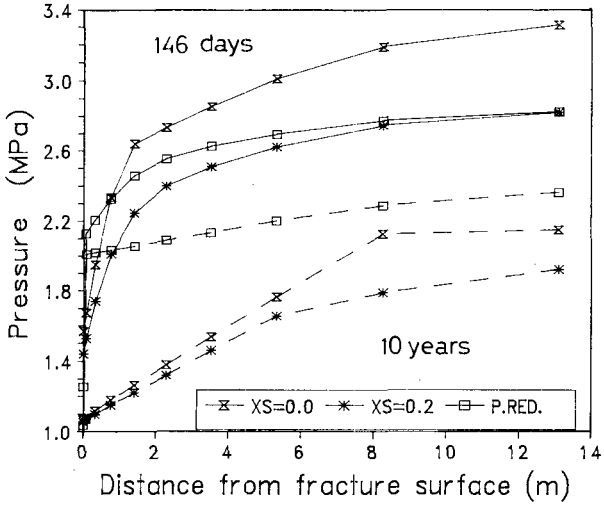

Figure 15. Pressure distribution as a function of distance from fracture at 146 days and 10 years in matrix block depletion problem.

reserves and the system is depleted after about 20 years, when all the matrix elements are in single-phase gas conditions. The same occurs for Case 2 after about 40 years. At this time the cumulative mass production for Case 1 and 2 are almost the same (Figure 14), as the initial reserves of pure water are almost the same. In fact the salt dissolved into the liquid phase is not recovered as the well produces steam from the beginning of exploitation. This is because the initial relative permeability to the liquid phase is low and the liquid phase is held by capillary forces in the matrix block. The introduction of permeability reduction in

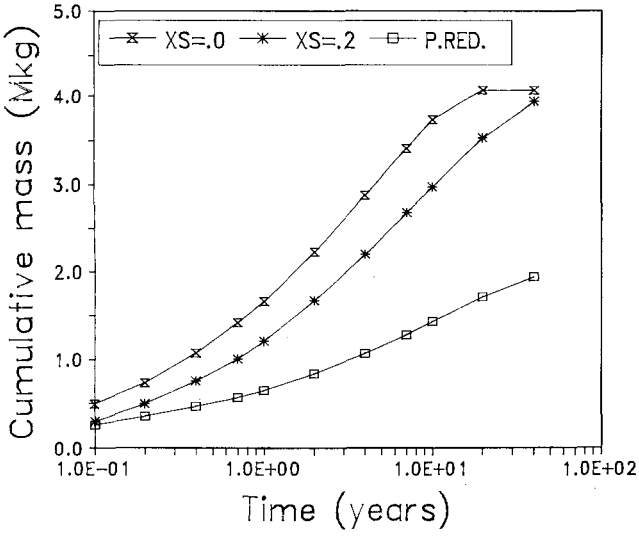

Figure 14. Cumulative fluid recovery as a function of time in matrix block depletion problem.

Case 3 is responsible for a faster decline in well production. After 40 years cumulative production for Case 3 is about 50% of that of Case 2.

For Case 3, after about 13 days the salt precipitation starts in the first matrix element. After 36.5 days, the solid saturation in this element is 0.11, causing a reduction of formation permeability to about 25% of its initial value. In both Case 2 and 3 the precipitation of solid salt close to the fracture surface continues as additional liquid phase flows towards the outermost element. There the vaporization produces the accumulation of sodium chloride and its precipitation. If the related permeability reduction is considered, the solid 'skin' at the fracture surface gives rise to a lower decrease of pressure in the interior of matrix block than in Case 2. Figure 15 shows the pressure distribution as a function of distance from the fracture surface after 146 days and 10 years, respectively. It is seen that when permeability reduction from solid precipitate is taken into account, most of the pressure drop occurs near the block surface.

After 40 years the well production for Case 3 is decreased by a factor of 1E+3. Even though about 50% of the original water reserves are still stored in the matrix block, they are produced only very slowly as the permeability of the outermost region of the matrix block is reduced to 0.6% of its initial value.

CONCLUSIONS

A thermophysical properties package for saline brines with non-condensible gas, that had been developed for a wellbore flow code "PROFILI", has been incorporated into the general-purpose multiphase fluid and heat flow

code TOUGH2. Our formulation includes a comprehensive suite of multiphase mixture effects, including density, viscosity, and enthalpy effects from salt dissolution, reduction in non-condensible gas solubility due to salinity, vapor pressure lowering due to salinity, and porosity and permeability reduction from the precipitation of salt.

Numerical simulations of reservoir depletion have demonstrated important effects from reduction in the solubility of non-condensible gas due to salinity. Vapor pressure lowering effects from salinity are very strong, and are likely to have a large impact on the depletion of vapor-dominated systems. In the depletion of fractured reservoirs, persistent boiling near the surfaces of matrix blocks will lead to concentration and ultimately precipitation of solids. This may cause a severe loss in permeability, and may considerably slow the rates at which fluid reserves can be recovered.

The simulation capabilities presented here will be of interest not only for geothermal reservoir studies, but also for analysis of fluid and heat flow conditions near high-level nuclear waste repositories.

ACKNOWLEDGEMENTS

This work was supported by Aquater S.p.A. of the Italian National Hydrocarbons Agency (ENI), by the International Institute for Geothermal Research of the Italian National Research Council (CNR), and by the Assistant Secretary for Conservation and Renewable Energy, Geothermal Division, of the U.S. Department of Energy under Contract No. DE-AC03-76SF00098. The authors would like to aknowledge the hospitality of the Institute for Fluid Mechanics, University of Hanover, Germany, where part of this work was performed.

NOMENCLATURE

$\mathbf{F}^{(i)}$ mass flux of component i, kg/(s m^2).
$\mathbf{g}$ acceleration of gravity, m^2/s.
k intrinsic permeability, m^2.
k_{rg} relative permeability to gas phase.
k_{rl} relative permeability to liquid phase.
k_b salting-out coefficient, kg/mol.
K_h Henry constant, Pa.
H specific enthalpy, J/kg.
m salt molality, mol/kg.
$M^{(i)}$ accumulation term of component i, kg/m^3.
$\mathbf{n}$ unit normal vector.
P pressure, Pa.
$Q^{(i)}$ source term for component i, kg/(s m^3).
R universal gas constant, J/(mol K).
S saturation.
T temperature, °C.
TK temperature, K.
V_n volume of grid element n, m^3.
$X^{(i)}$ mass fraction of component i.
$Y^{(3)}$ mole fraction of NCG.
$W^{(3)}$ molecular weight of NCG, kg/mol.
Γ_n surface area of grid element n, m^2.
ϕ porosity.
μ dynamic viscosity, Pa s.
ρ density, kg/m^3.

Subscripts and Superscripts

b brine.
boil boiling.
eq equivalent salt mass fraction.
g gas phase.
l liquid phase.
s solid salt phase.
sat vapor-saturated.
sol halite solubility.
1 water component, H_2O.
2 salt component, NaCl.
3 gas component, NCG.

REFERENCES

Battistelli, A., "PROFILI code: the thermodynamical package for H_2O-NaCl-CO_2 fluid mixtures". Unpublished Aquater report H 6046, Nov., 1991.

Chierici, G. L., Giannone, G., and Sclocchi G., "A Wellbore Model for Two-Phase Flow in Geothermal Reservoirs". SPE 10315, 1981.

Chou, I.- M., "Phase relations in the system NaCl-KCl-H_2O. III : Solubilities of halite in vapor-saturated liquids above 445 °C and redetermination of Phase equilibrium properties in the system NaCl-H_2O". Geoch. et Cosm. Acta, Vol. 51, pp. 1965-1975, 1987.

Cramer, S. D., "The solubility of methane, carbon dioxide and oxigen in brines from 0° to 300 °C". US Bureau of Mines, report No. 8706, 1982.

D'Amore, F., and Truesdell, A. H., "A rewiew of solubilities and equilibrium constants for gaseous species of geothermal interest". Sci. Geol. Bull., 41, 3-4, pp. 309-332, Strasbourg, 1988.

Deer, W. A., Howie, R. A., and Zussman, J., "An Introdution to the Rock-Forming Minerals". Longman Group Limited, London, 1966.

Gudmundsson, J.- S., and Thrainsson H., "Power potential of two-phase geothermal wells". Geothermics, Vol. 18, No. 3, pp 357-366, 1989.

Haas, J. L. Jr., "Physical Properties of the Coexisting Phases and Thermodynamical Properties of the H_2O Component in Boiling NaCl Solutions". USGS Bulletin

1421-A, 1976.

Himmelblau, D. M., "Partial molal heats and entropies of solution for gases dissolved in water from the freezing to the near critical point". J. Phys. Chem., Vol. 63, pp. 1803-1808, 1959.

International Formulation Committe, "A Formulation of the Thermodynamic Properties of Ordinary Water Substance". IFC Secretariat, Düsseldorf, Germany, 1967.

Michaelides, E. E., "Thermodynamic properties of geothermal fluids". GRC Transactions, Vol. 5, Oct. 1981.

O'Sullivan, M. J., Bodvarsson, G. S., Pruess, K., and Blakeley, M. R., "Fluid and Heat Flow in Gas-Rich Geothermal Reservoirs". SPE J., pp. 215-226, Apr. 1985.

Palaban, R. T., and Pitzer, K. S., "Thermodynamics of concentrated electrolyte mixtures and the prediction of mineral solubilities to high temperatures for mixtures in the system Na-K-Mg-Cl-SO_4-OH-H_2O". Geoch. et Cosm. Acta, Vol. 51, pp.2429-2443, 1987.

Pritchett, J. W., Rice, M. H., and Riney T. D., "Equation-of-state for water-carbon$_3$ dioxide mixtures: implications for Baca reservoir". S^3 report SSS-R-81-4870, report DOE/ET/27163-8, UC-66a, Feb. 1981.

Pruess, K., "Development of the General Purpose Simulator MULKOM". Annual report 1982, Earth Sci. Div., Lawrence Berkeley Lab. report, LBL-15500, Berkeley, CA, 1983.

Pruess, K. and Narashiman, T. N., "A Practical Method for Modeling Fluid and Heat Flow in Fractured Porous Media". Soc. Pet. Eng. J., Vol. 25, N. 1, pp. 14-26, 1985.

Pruess, K., "TOUGH2 - A General-Purpose Numerical Simulator for Multiphase Fluid and Heat Flow", Earth Sci. Div., Lawrence Berkeley Lab. report LBL-29400, Berkeley, CA, 1991a.

Pruess, K., "EOS7 - An Equation-of-State Module for the TOUGH2 Simulator for Two-Phase Flow of Saline Water and Air", Earth Sci. Div., Lawrence Berkeley Lab. report LBL-31114, Berkeley, CA, 1991b.

Pruess, K., and O'Sullivan, M., "Effects of Capillarity and Vapor Adsorption in the Depletion of Vapor-Dominated Geothermal Reservoirs". 17th Workshop on Geoth. Res. Eng., Stanford University, Stanford, CA, Jan., 29-31, 1992.

Silvester, L. F., and Pitzer, K. S., "Thermodynamics of geothermal brines - I. Thermodynamic properties of vapor-saturated NaCl (aq) solutions from 0-300 °C". Lawrence Berkeley Lab. report LBL-4456, UC-66, TID-4500-R64, 1976.

Sutton, F. M., and McNabb, A., "Boiling Curves at Broadlands Field". New Zealand J. of Sci., Vol. 20, pp. 333-337, 1977.

Verma, A., and Pruess, K., "Thermohydrological Conditions and Silica Redistribution Near High-Level Nuclear Wastes Emplaced in Saturated Geological Formations". J. of Geophys. Res., Vol.93, No. B2, pp. 1159-1173, Feb. 10, 1988.